

# Solid-State $^{51}\text{V}$ NMR Structural Studies on Supported Vanadium(V) Oxide Catalysts: Vanadium Oxide Surface Layers on Alumina and Titania Supports

Hellmut Eckert\*

Department of Chemistry, University of California, Santa Barbara, Goleta, California 93106

and Israel E. Wachs

Zettlemoyer Center for Surface Studies and Department of Chemical Engineering, Lehigh University, Bethlehem, Pennsylvania 18015 (Received: February 3, 1989)

Solid-state wide-line, magic-angle spinning (MAS) and pulse excitation (nutating) NMR techniques are applied in a study of local environments in two-dimensional vanadium(V) oxide surface layers on titania and alumina supports. Two main surface vanadium oxide species with different bonding environments are detected, which are, on the basis of their anisotropic chemical shift and nuclear electric quadrupolar coupling properties, assigned to 4- and 6-coordinate V-O environments. In all materials, the relative amount of 6-coordinate surface species increases monotonically as a function of the vanadium oxide surface coverage. However, the results indicate a marked dependence of the surface vanadium oxide structure on the metal oxide support material. Vanadium(V) oxide on  $\text{TiO}_2$  (anatase) substrates displays the highest tendency to be 6-coordinated down to very low surface coverages. Hydrous species (OH and  $\text{H}_2\text{O}$ ) participate in this environment, and upon dehydration in vacuo, a new tetrahedral species is formed. These results illustrate the suitability of  $^{51}\text{V}$  NMR as a unique quantitative spectroscopic tool in the structural analysis of vanadium(V) oxide catalytic materials.

## Introduction

Fundamental research investigations of the past few years have revealed that multicomponent metal oxide systems may interact at interfaces by having one component form a two-dimensional metal oxide overlayer on the second metal oxide component.<sup>1-6</sup> Catalytic systems of considerable interest as models for the analysis of interactions at the metal oxide/metal oxide interface are the  $\text{V}_2\text{O}_5/\text{TiO}_2$  and  $\text{V}_2\text{O}_5/\text{Al}_2\text{O}_3$  systems.<sup>7-29</sup>

Many recent studies have shown that supported  $\text{V}_2\text{O}_5/\text{TiO}_2$  (anatase) is a superior catalyst to unsupported crystalline  $\text{V}_2\text{O}_5$  catalysts for the selective oxidation of hydrocarbons.<sup>7-18</sup> The two-dimensional overlayers of surface vanadium oxide species on the titania support were found to be the active sites for these partial oxidation reactions and to possess a higher activity and selectivity than crystalline  $\text{V}_2\text{O}_5$ . In addition, the  $\text{TiO}_2$  (anatase) support must be covered by a complete monolayer of the surface vanadium oxide species since exposed titania sites lead to the undesired combustion of the partial oxidation products.

The mechanism by which  $\text{TiO}_2$  (anatase) modifies the properties of the supported  $\text{V}_2\text{O}_5$  phase is not well understood. It has been argued that the special properties of  $\text{V}_2\text{O}_5/\text{TiO}_2$  (anatase) arise from the close structural similarities between the oxides in the bulk and preferential exposure of the (010) plane of small  $\text{V}_2\text{O}_5$  platelets that contain perpendicular-oriented  $\text{V}_2\text{O}_5$  groups.<sup>19,20</sup> Neither of these studies, however, contain any direct structural measurements of the supported vanadium oxide phase, whose amorphous nature requires the use of characterization methods that provide short range order structural information.

Direct structural measurements of the supported vanadium oxide phase on  $\text{TiO}_2$  by laser Raman spectroscopy and X-ray absorption spectroscopy indeed reveal that the structure of the supported vanadium oxide phase is different from that of bulk  $\text{V}_2\text{O}_5$ , consisting of a two-dimensional metal oxide overlayer, in which more than one surface vanadium oxide species appears to

(1) Haber, J. In *Surface Properties and Catalysis by Non-Metals*; Bonnelle, J. P., et al., Eds.; Reidel: Dordrecht, The Netherlands, 1983; p 1.

(2) Haber, J. *Proceedings of the 8th International Congress on Catalysis*; Dechema-Chemie Verlag: West Berlin, 1984; Vol. 1, p 185.

(3) Haber, J. *Pure Appl. Chem.* **1984**, *56*, 1663.

(4) Wachs, I. E.; Hardcastle, F. D.; Chan, S. S. *Spectroscopy (Eugene, Oreg.)* **1986**, *1*, 30.

(5) Dixit, L.; Gerrard, D. L.; Bowley, H. *Appl. Spectrosc. Rev.* **1986**, *22*, 189.

(6) Bartlett, J. R.; Cooney, R. P. In *Spectroscopy of Inorganic-Based Materials*; Clark, R. J. H., Hester, R. E., Eds.; Wiley: New York, 1987; p 187.

(7) VanHove, D.; Blanchard, M. *Bull. Soc. Chim. Fr.* **1971**, 3291.

(8) Grabowski, R.; Grzybowska, B.; Haber, J.; Sloczynski, J. *React. Kinet. Catal. Lett.* **1975**, *2*, 81.

(9) Gasiot, I.; Gasiot, M.; Grzybowska, B.; Kozlowski, R.; Sloczynski, J. *Bull. Acad. Pol. Sci., Ser. Sci. Chim.* **1979**, *27*, 829. Gasiot, M.; Grzybowska, B. *Ibid.* **1979**, *27*, 835.

(10) Bond, G. C.; Sarkany, J.; Parfitt, G. D. *J. Catal.* **1979**, *57*, 476.

(11) Murakami, Y.; Inomata, M.; Miyamoto, A.; Mou, K. *Proceedings of the 7th International Congress on Catalysis*; 1980; p 1344.

(12) Bond, G. C.; Konig, P. J. *J. Catal.* **1982**, *77*, 309. Bond, G. C.; Bruckman, K. *Faraday Discuss. Chem. Soc.* **1981**, *72*, 235.

(13) Van Hengstum, A. J.; Van Ommen, J. G.; Bosch, H.; Gellings, P. J. *Appl. Catal.* **1983**, *8*, 369.

(14) Gasiot, M.; Gasiot, I.; Grzybowska, B. *Appl. Catal.* **1984**, *10*, 87.

(15) Wachs, I. E.; Saleh, R. Y.; Chan, S. S.; Chersich, C. C. *Appl. Catal.* **1985**, *15*, 339.

(16) Wachs, I. E.; Chan, S. S.; Saleh, R. Y. *J. Catal.* **1985**, *91*, 366.

(17) Saleh, R. Y.; Wachs, I. E.; Chan, S. S.; Chersich, C. C. *J. Catal.* **1986**, *98*, 102.

(18) Gasiot, M.; Haber, J.; Machej, T. *Appl. Catal.* **1987**, *33*, 1.

(19) Vejux, A.; Courtine, P. *J. Solid State Chem.* **1978**, *23*, 93. Courtine, P.; Vejux, A. C. R. *Seances Acad. Sci., Ser. C* **1978**, *286*, 135.

(20) Inomata, M.; Mori, K.; Miyamoto, A.; Ui, T.; Murakami, Y. *J. Phys. Chem.* **1983**, *87*, 754.

(21) Roozeboom, F.; Mittlemeijer-Hazeleger, M. C.; Mouljn, J. A.; Medema, J.; deBeer, V. H. J.; Gellings, P. J. *J. Phys. Chem.* **1980**, *84*, 2783.

(22) Kozlowski, R.; Pettifer, R. F.; Thomas, J. M. *J. Phys. Chem.* **1983**, *87*, 5176.

(23) Wachs, I. E.; Chan, S. S. *Appl. Surf. Sci.* **1984**, *20*, 181. Chan, S. S.; Wachs, I. E.; Murrell, L. L.; Wang, L.; Hall, W. K. *J. Phys. Chem.* **1984**, *88*, 5381.

(24) Haber, J.; Kozlowska, A.; Kozlowski, R. *J. Catal.* **1986**, *102*, 52.

(25) Wachs, I. E.; Hardcastle, S. D.; Chan, S. S. *Mater. Res. Soc. Symp. Proc.* **1988**, *111*, 353.

(26) Haber, J.; Kozlowska, A.; Kozlowski, R. *Hydroprocessing Zeolites and Catalytic Processes. Proceedings of the 9th International Congress on Catalysis*, Calgary; Phillips, M. J., Ternan, M., Eds.; 1988, p 1481.

(27) Hardcastle, F. D.; Wachs, I. E. *Proceedings of the 9th International Congress on Catalysis, Calgary, 1988*; Phillips, M. J., Ternan, M., Eds.; Vol. 3, p 1449.

(28) Inomata, M.; Mori, K.; Miyamoto, A.; Murakami, Y.; *J. Phys. Chem.* **1983**, *87*, 761.

(29) Yoshida, S.; Tanaka, T.; Nishimura, Y.; Mizutani, H.; Funabiki, T. *Proceedings of the 9th International Congress on Catalysis, Calgary, 1988*; Phillips, M. J., Ternan, M., Eds.; Vol. 3, p 1473.

be present.<sup>15-17,21-27</sup> The strong contribution of the  $\text{TiO}_2$  (anatase) signal to the Raman spectrum, however, makes it difficult to make a complete structural determination of the surface vanadium oxide species solely on Raman spectroscopy. X-Ray absorption spectroscopy (EXAFS/XANES) of the  $\text{V}_2\text{O}_5/\text{TiO}_2$  (anatase) system has provided structural information concerning bond lengths and coordination numbers.<sup>22,24,26</sup> These studies concluded that the two-dimensional vanadium oxide overlayer is composed of isolated tetrahedral surface vanadate species attached to the titania support and that the surface vanadium oxide species are disordered.<sup>22,24</sup> The unique catalytic properties have been attributed to this intrinsic disorder.<sup>22</sup> As to the detailed bonding state of the vanadium(V) oxide on  $\gamma$ -alumina surfaces, the proposals have been conflicting, ranging from "small disordered  $\text{V}_2\text{O}_5$  particles,"<sup>28</sup> monodispersed  $\text{VO}_2\text{O}_{2/2}$  ("metavanadate groups"),<sup>27,29</sup> and dimeric  $\text{V}_2\text{O}_7$  ("pyrovanadate groups")<sup>24</sup> to an "inactive" 3-coordinate species acting as a Brønsted site.<sup>28</sup> However, many of the above studies have suffered from the considerable disorder present as well as from the inherent difficulty to provide quantitative species concentrations from signal intensities. Furthermore, it is not always clear whether the structural assignments made in the literature refer to ambient samples or samples with dehydrated surfaces.

Solid-state NMR methods represent a novel and promising approach to these systems. Since only the local environment of the nucleus under study is probed by NMR, this method is well suited for the structural analysis of disordered systems such as the two-dimensional surface vanadium oxide phases of interest in the present study, in which the lack of long-range order precludes the application of standard diffraction methods. In addition to the structural information provided by NMR methods, the direct proportionality of the signal intensity to the number of contributing nuclei makes NMR a useful technique for quantitative studies. While  $^{27}\text{Al}$ ,  $^{29}\text{Si}$ , and  $^1\text{H}$  MAS NMR have found widespread applications in catalytic systems,<sup>30</sup> including the ones of the present study,<sup>31</sup> the scope of previous  $^{51}\text{V}$  NMR applications to problems in materials science, such as structural studies of catalysts or catalyst-analogue systems, has been extremely limited.<sup>32-37</sup> This is especially surprising in view of the highly favorable NMR properties of the  $^{51}\text{V}$  isotope, which is 99.76% naturally abundant and has a large magnetic moment and short spin-lattice relaxation times due to the nuclear electric quadrupole interaction ( $I = 7/2$ ). In a recent paper by Le Costumer et al., the pH dependence of the  $^{51}\text{V}$  NMR spectra on impregnated aluminas in the wet, dried, and cured state has been investigated,<sup>36</sup> but to date, no systematic studies of the effect of different metal oxide supports or surface coverages have been carried out. Recently, within the context of preliminary investigations on  $\text{V}_2\text{O}_5/\text{Al}_2\text{O}_3$  catalysts and model compounds,<sup>35</sup> we highlighted the ability of the anisotropic  $^{51}\text{V}$  chemical shielding properties in providing structural information. In this contribution, the local environment of supported pentavalent vanadium oxide, dispersed on  $\text{TiO}_2$  (anatase),  $\text{TiO}_2$  (rutile), and  $\text{TiO}_2$  (Degussa P-25), as well as  $\gamma$ - $\text{Al}_2\text{O}_3$  will be discussed on the basis of comprehensive solid-state wide-line, magic-angle spinning and pulse excitation (nutration) NMR studies undertaken on these systems and a variety of crystalline model compounds. The influence of vanadium oxide surface coverage, the nature of the oxide support, and the extent of hydration upon the structure of the supported vanadium oxide phases will be of particular interest.

(30) Duncan, T. M.; Dybowski, C. R. *Surf. Sci. Rep.* **1981**, *1*, 157.

(31) McMillan, M.; Brinen, J. S.; Haller, G. L. *J. Catal.* **1986**, *97*, 243.

(32) Mastikhin, V. M.; Lapina, O. B.; Krasilnikov, V. N.; Ivakin, A. A. *React. Kinet. Catal. Lett.* **1984**, *24*, 119.

(33) Mastikhin, V. M.; Lapina, O. B.; Simonova, L. G. *React. Kinet. Catal. Lett.* **1984**, *24*, 127.

(34) Gorskova, T. P.; Maksimovskaya, R. I.; Tarasova, D. V.; Chumachenko, N. N.; Nikoro, T. A. *React. Kinet. Catal. Lett.* **1984**, *24*, 107.

(35) Eckert, H.; Wachs, I. E. *Mater. Res. Soc. Symp. Proc.* **1988**, *111*, 455.

(36) Le Costumer, L. R.; Taouk, B.; Le Meur, M.; Payen, E.; Guelton, M.; Grimblot, J. *J. Phys. Chem.* **1988**, *92*, 1230.

(37) Taouk, B.; Guelton, H.; Grimblot, J.; Bonnelle, J. P. *J. Phys. Chem.* **1988**, *92*, 6700.

## Fundamental Concepts and Methodology

The  $^{51}\text{V}$  isotope has spin  $7/2$  and consequently possesses a nuclear electric quadrupole moment. Therefore, NMR spectra in the solid state are affected by the interaction of this moment with electrostatic field gradients created by asymmetric electronic environments. For  $^{51}\text{V}$ , those quadrupolar interactions are of moderate strength and can be treated by simple first- or second-order perturbation theory.<sup>38</sup> Provided that  $H_z > 20H_Q$ , i.e., the nuclear magnetic spin interaction energy exceeds that of the quadrupolar interaction substantially, a first-order perturbation treatment is sufficient. Under these circumstances, the resonance line is split into seven lines, one of which (the central  $+1/2 \rightarrow -1/2$  transition) remains unaffected by the quadrupolar interaction.<sup>38</sup> This transition is symmetrically surrounded by six "satellite" transitions, which exhibit typical powder patterns arising from an isotropic distribution of the electric field gradient tensor principal-axis direction with respect to the external magnetic field. In addition, all transitions are affected by the chemical shift anisotropy. Magic-angle spinning affords a straightforward way of determining the isotropic chemical shift from the position of the narrowed central transition. On the other hand, the three principal components of the shielding tensor are available from singularities in the nonspinning spectrum or from an analysis of the spinning sideband patterns under conditions of slow magic-angle spinning.<sup>39</sup>

If the above condition is not satisfied, the quadrupolar perturbation treatment has to be extended to second order. This will affect the central  $+1/2 \rightarrow -1/2$  transition, resulting in more complicated powder patterns that reflect the symmetry of the electric field gradient tensor.<sup>38</sup> The line shape will now depend on the shielding tensor, the nuclear electric quadrupole tensor components, and the three Euler angles that specify the relative orientation of both tensors with respect to each other. In general, it will be impossible to deduce all of these quantities unambiguously from powder spectra. On the other hand, an independent piece of information on the strength of the quadrupolar interaction can be obtained from field-dependent MAS-NMR: For second-order perturbations, the quantization axis of the  $^{51}\text{V}$  nuclear spins will deviate from the magnetic field direction. Consequently, line narrowing by MAS is incomplete and will improve proportional to the strength of the external magnetic field. In addition, the resonance position is affected by a second-order quadrupolar shift  $\delta^{(2)}$ ,<sup>40</sup> such that  $\delta_{\text{exp}} = \delta_{\text{iso}} + \delta^{(2)}$ . For a spin- $7/2$  nucleus, this second-order quadrupolar shift amounts to

$$\delta^{(2)} \text{ (ppm)} = -2551\nu_0^{-2}(e^2qQ/h)^2(1 + \eta^2/3)$$

where  $\nu_0$  is the nuclear Larmor precession frequency in cps and  $e^2qQ/h$  and  $\eta$  are the principal component and the asymmetry parameter, respectively, of the nuclear electric quadrupolar interaction.

The effect of chemical shift and nuclear electric quadrupolar interactions on the  $^{51}\text{V}$  NMR line shape can thus be assessed quantitatively by measurements at different field strengths. At higher magnetic fields, second-order effects upon line position and shape are minimized.

The excitation spectrum of the  $^{51}\text{V}$  nucleus provides additional, independent information about the quadrupole interaction. Under standard experimental conditions, the Fourier spectrum of a radio-frequency pulse has no or insufficient intensity to excite outer quadrupolar satellites, that are too far off resonance ( $> \sim 300$  kHz). As a result, the effective precession frequencies of the  $^{51}\text{V}$  nuclei in the rotating frame are increased.<sup>41,42</sup> When a fictitious spin- $1/2$  formalism is used,<sup>43</sup> it has been shown that in the limiting

(38) Cohen, M. H.; Reif, F. In *Solid State Physics*; Seitz, Turnbull, Eds.; Academic Press: New York, 1957; Vol. 5, p 321.

(39) Herzfeld, J.; Berger, A. E. *J. Chem. Phys.* **1980**, *73*, 6021.

(40) Freude, D.; Haase, J.; Klinowski, J.; Carpenter, T. A.; Ronikier, G. *Chem. Phys. Lett.* **1985**, *119*, 365.

(41) Samoson, A.; Lippmaa, E. *Phys. Rev. B* **1983**, *28*, 6567.

(42) Kentgens, A. P. M.; Lemmens, J. J. M.; Geurts, F. M. M.; Veeman, W. S. *J. Magn. Reson.* **1987**, *71*, 62.

(43) Vega, S. *J. Chem. Phys.* **1978**, *68*, 5518. Wokaun, A.; Ernst, R. R. *J. Chem. Phys.* **1977**, *67*, 1752.

case of entirely selective irradiation of the central  $+1/2 \rightarrow -1/2$  transition of a half-integer quadrupolar nucleus with spin quantum number  $I$ , the effective precession frequency is increased by the factor  $(I + 1/2)$ , resulting in a corresponding shortening of the  $90^\circ$  pulse length.<sup>44</sup> Therefore, systematic measurements of signal intensities as a function of pulse length, commonly called "pulse excitation" or "nutating NMR studies", can be used to determine the degree of excitation selectivity. Such experiments, which differentiate with respect to the strength and symmetry of the nuclear electric quadrupolar interaction tensor, have been exploited in this study as an additional tool of site identification and spectral editing. Knowledge of the excitation behavior is also required for quantitative NMR studies, since the signal intensity also depends on the degree of excitation selectivity.<sup>45</sup>

### Experimental Section

**Sample Preparation and Characterization.** The supported vanadium oxide on  $\text{TiO}_2$  catalysts were prepared by the incipient wetness impregnation method with  $\text{VO}(\text{OC}_2\text{H}_5)_3$  in ethanol on anatase (surface area  $80 \text{ m}^2/\text{g}$ ), rutile (surface area  $25 \text{ m}^2/\text{g}$ ), and commercial titania (Degussa P-25, surface area  $50 \text{ m}^2/\text{g}$ ; anatase/rutile ratio ca. 2). The anatase sample was prepared by hydrolysis of titanium isopropoxide and the rutile sample was prepared by hydrolysis of  $\text{TiCl}_4$ . The impregnated samples were subsequently dried at room temperature for 16 h and dried at  $110\text{--}120^\circ\text{C}$  for 16 h. Subsequently, the anatase and rutile samples were calcined at  $350^\circ\text{C}$  and the Degussa samples were calcined at  $450^\circ\text{C}$  for 2 h to form the supported vanadium oxide on  $\text{TiO}_2$  catalysts. Vanadia contents were determined by ICP analysis. For the  $\text{V}_2\text{O}_5/\text{TiO}_2$  (Degussa) catalysts, Raman characterization revealed that samples with up to 7 wt %  $\text{V}_2\text{O}_5$  contain only surface vanadium oxide species; above this limit,  $\text{V}_2\text{O}_5$  crystallites were observed as an additional phase. According to this experimental result, the surface coverage was defined operationally to be 1.0 for 7%  $\text{V}_2\text{O}_5/\text{TiO}_2$  (Degussa), and surface coverages for other samples were derived accordingly. Assuming an average V-V distance of  $3.4 \text{ \AA}$  (in  $\text{NH}_4\text{VO}_3$ ) on the surface, a  $\text{V}_2\text{O}_5$  monolayer would actually correspond to only 3.3 wt %  $\text{V}_2\text{O}_5$  on a  $50 \text{ m}^2/\text{g}$  surface area. It therefore appears that the vanadium oxide surface species is forming double layers before surface crystallization of  $\text{V}_2\text{O}_5$ . Analogous characterization was carried out for the anatase- and rutile-based samples. TGA studies on the  $\text{V}_2\text{O}_5/\text{TiO}_2$  (Degussa) samples, using a Du Pont Model 951 thermogravimetric balance, indicate a ca. 2% weight loss due to desorption of water between room temperature and ca.  $300^\circ\text{C}$ ; up to  $800^\circ\text{C}$ , no further significant weight loss was observed.

The supported vanadium oxide on  $\text{Al}_2\text{O}_3$  catalysts were prepared by the incipient wetness impregnation method with  $\text{VO}(\text{OC}_3\text{H}_7)_3$  in methanol on Harshaw  $\text{Al}_2\text{O}_3$  (surface area  $180 \text{ m}^2/\text{g}$ ). The impregnated samples were subsequently dried at room temperature for 16 h, dried at  $110\text{--}120^\circ\text{C}$  for 16 h, and calcined at  $500^\circ\text{C}$  for 16 h to form the supported catalysts. The various calcination temperatures and times were selected to minimize shrinkage of the surface areas of the alumina and titania support materials. Vanadia contents were determined by ICP analysis. Raman characterization of the  $\text{V}_2\text{O}_5/\text{Al}_2\text{O}_3$  system revealed that the 1–20%  $\text{V}_2\text{O}_5/\text{Al}_2\text{O}_3$  samples contained only molecularly dispersed surface vanadium oxide species and that at higher vanadia contents  $\text{V}_2\text{O}_5$  crystallites are observed in addition to the molecularly dispersed surface species. According to this experimental result, the surface coverage was defined operationally to be 1.0 for the 20 wt %  $\text{V}_2\text{O}_5/\text{Al}_2\text{O}_3$  sample, and the surface coverages for the other samples were derived accordingly. As in the case of  $\text{V}_2\text{O}_5$  on titania, the vanadium(V) surface species appears to form a double layer. TGA studies indicate a ca. 10% weight loss due to desorption of water between room temperature and ca.  $300^\circ\text{C}$ , whereupon no further weight loss occurred up to  $800^\circ\text{C}$ . For representative compositions, samples were dehydrated at tem-

peratures between  $150$  and  $400^\circ\text{C}$  for  $0.5\text{--}1$  h in a  $10^{-3}$ -Torr vacuum and studied by NMR within flame-sealed containers. Within the limits specified, the  $^{51}\text{V}$  NMR spectra showed little dependence on the dehydration conditions.

**Nuclear Magnetic Resonance Studies.** Room-temperature wide-line and MAS solid-state NMR measurements were carried out with a General Electric Model GN-300 spectrometer, equipped with an Explorer high-speed digitizer and a 7-mm multinuclear MAS-NMR probe (zirconia stator and spinners) from Doty Scientific. The pulse excitation behavior was mapped out on nonspinning samples by systematic signal intensity measurements as a function of pulse lengths (32 increments of  $0.5 \mu\text{s}$  at an rf field strength of  $35.7 \text{ kHz}$ ), with recycle delays of  $1\text{--}2$  min, which were found sufficiently long to eliminate any saturation effects on line intensities. For samples with wide-line spectra that were either too broad or contained spectral interferences, the pulse excitation behavior was studied under MAS conditions, sampling the FID in synchrony with the specimen rotation. Although the results obtained under wide-line and MAS conditions are generally not identical,<sup>42</sup> our results of parallel studies on several model compounds with widely different excitation behaviors indicate that such deviations are much more pronounced in the long-term behavior and do not significantly affect the experimentally measured effective  $90^\circ$  pulse length.

For all the catalyst samples, the  $90^\circ$  pulse length is shortened from 7 (in  $\text{VOCl}_3$ ) to  $2.4\text{--}3.3 \mu\text{s}$ . In the limiting case of entirely selective excitation of the central  $+1/2 \rightarrow -1/2$  transition, the effective  $90^\circ$  pulse length would be shortened to  $1/(I + 1/2) = 1/4$  of its value in the liquid state, i.e.,  $1.75 \mu\text{s}$ . Our results thus indicate that outer quadrupolar satellite transitions are also being partially excited. To avoid signal distortions from varying degrees of selectivity across the NMR powder pattern and to enable quantitative studies, all spectra were obtained with pulses of  $0.5\text{--}1\text{-}\mu\text{s}$  length, where line shapes and peak area ratios are expected to be independent of the pulse length;<sup>41</sup> this was also verified by experiment. Spectra were typically obtained with a simple one-pulse sequence (Bloch decay), a preacquisition delay of  $10 \mu\text{s}$ , dwell time of  $1\text{--}2 \mu\text{s}$ , relaxation delays of  $1\text{--}5$  s, and 1K data points. Although the use of Bloch decays bears the potential danger of producing somewhat distorted line shapes, it is the preferred method here, since it avoids complications arising from varying degrees of excitation selectivity that become important with the longer pulse length needed to generate  $90^\circ$  and  $180^\circ$  pulses for spin echoes. All chemical shifts are referenced against liquid  $\text{VOCl}_3$ , with use of a spinning sample of solid vanadinite ( $\text{Pb}_5(\text{VO}_4)_3\text{Cl}$ ,  $\delta = -509 \text{ ppm}$  at  $7.05 \text{ T}$ ) as a secondary reference material. To investigate the field dependence, additional measurements were taken at  $131.48 \text{ MHz}$  ( $11.7 \text{ T}$ ), with a GN-500 spectrometer equipped with a 5-mm Doty probe, and at  $52.6 \text{ MHz}$  ( $4.7 \text{ T}$ ) with a home-built 5-mm wide-line NMR probe and a modified 7-mm CPMAS Doty probe on a wide-bore system at the Southern California Regional NMR Facility. Measurements at the lower field strength were hampered by an overlapping  $^{23}\text{Na}$  signal arising from probe background.  $^1\text{H}$  MAS-NMR spectra were obtained at  $300 \text{ MHz}$  on a Nicolet Model NT-300 spectrometer, with a specially designed high-speed spinning Doty probe with minimum proton background. Chemical shifts are referenced against liquid tetramethylsilane.

### Results, Analysis, and Interpretation

Since the  $^{51}\text{V}$  isotope has a moderately large nuclear electric quadrupole moment, wide-line  $^{51}\text{V}$  NMR spectra can be quite complex due to the simultaneous line-broadening effects arising from second-order quadrupolar and chemical shift anisotropy interactions. Both interactions can be separated, however, due to their opposite dependence on the strength of the applied magnetic field.<sup>46</sup> Figure 1, which shows the field dependence for two representative catalyst samples, clearly shows that the spectra are significantly broader at higher fields, hence confirming

(44) Man, P. P.; Theveneau, H.; Papon, P. *J. Magn. Reson.* **1985**, *64*, 271.

(45) Fenzke, D.; Freude, T.; Fröhlich, T.; Haase, J. *Chem. Phys. Lett.* **1984**, *111*, 171.

(46) Baugher, J. F.; Taylor, P. C.; Oja, T.; Bray, P. J. *J. Chem. Phys.* **1969**, *50*, 4914.

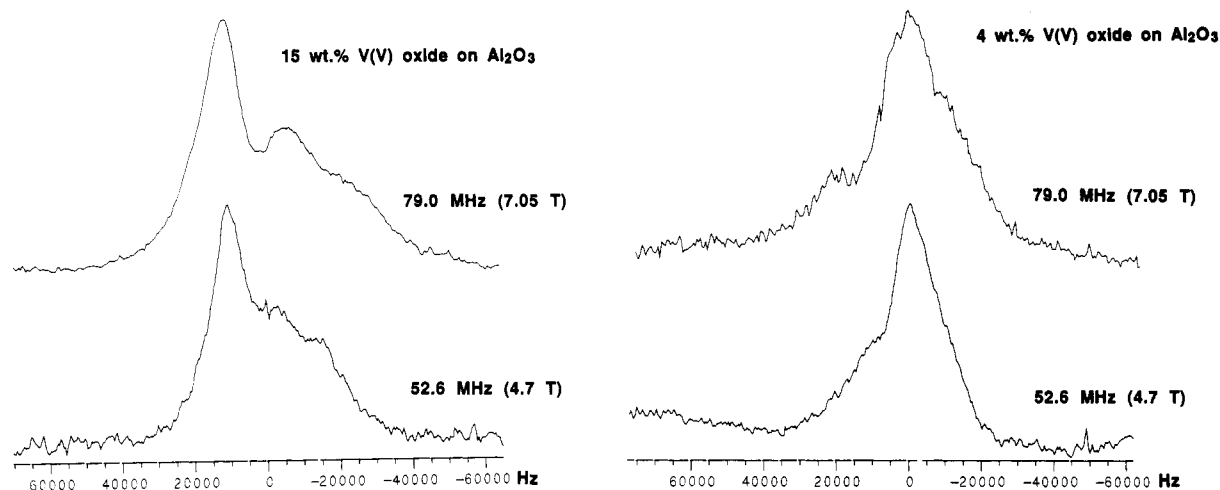


**Figure 1.** 79.0-MHz (7.05-T) and 52.6-MHz (4.65-T)  $^{51}\text{V}$  wide-line NMR spectra of representative catalyst samples for illustration of the influence of the external magnetic field strength on the  $^{51}\text{V}$  NMR line shape. Note that the pattern observed at the higher field strength is significantly wider, confirming the dominance of the chemical shift anisotropy on the line shape.

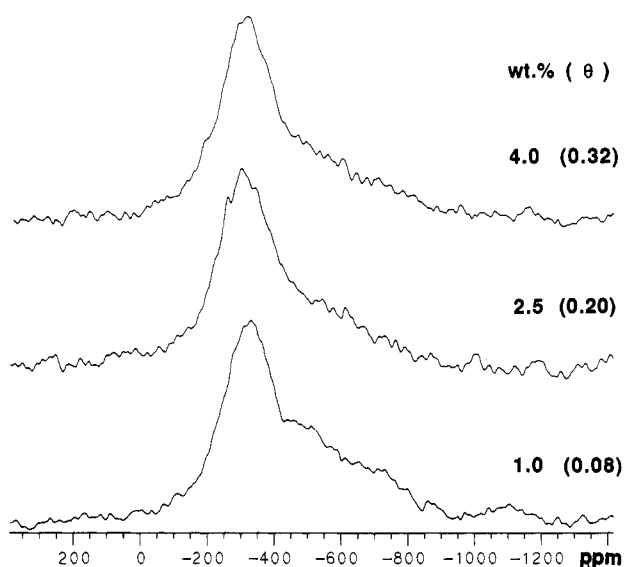


**Figure 2.** 79.0-MHz  $^{51}\text{V}$  wide-line NMR spectra of  $\text{V}_2\text{O}_5$  on anatase. The numerals indicate the overall concentration and the surface coverage of  $\text{V}_2\text{O}_5$  (in parentheses).

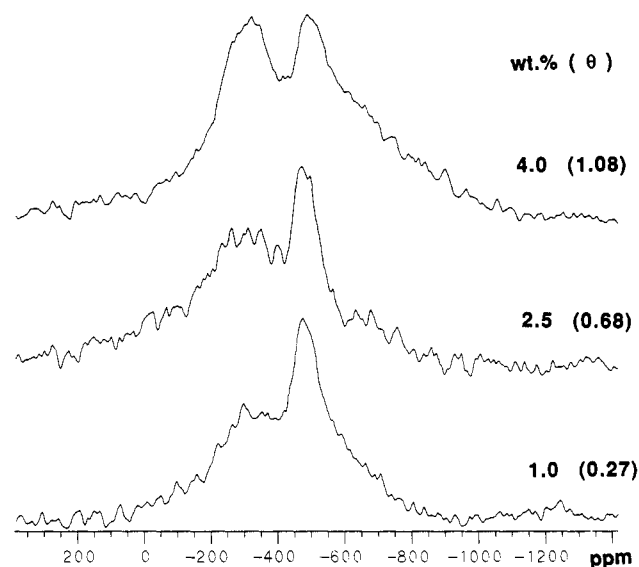


**Figure 3.** 79.0-MHz  $^{51}\text{V}$  wide-line NMR spectra of  $\text{V}_2\text{O}_5$  on rutile. The numerals indicate the overall concentration and the surface coverage of  $\text{V}_2\text{O}_5$  (in parentheses).

that the line shapes are dominated by chemical shift anisotropy and distribution rather than second-order quadrupolar effects. This finding agrees with earlier results on both 4- and 6-coordinated vanadium(V) oxide model compounds.<sup>47-49</sup> To minimize the influence of second-order quadrupolar effects, most of our studies were carried out at the higher field strength of 7.05 T.

Figures 2-5 show the wide-line NMR spectra of vanadium(V) oxide/ $\text{TiO}_2$  (anatase), vanadium(V) oxide/ $\text{TiO}_2$  (rutile), vanadium(V) oxide/ $\text{TiO}_2$  (Degussa), and vanadium(V) oxide/ $\gamma\text{-Al}_2\text{O}_3$  catalyst samples, respectively, at ambient conditions, as a function of vanadia content and surface coverage  $\theta$ . Although they show a striking dependence on the nature of the support material, all spectra can be essentially interpreted in terms of two principal signal components: "type a" (generally favored at high coverages) and "type b" (generally favored at low surface coverages). These two vanadium(V) oxide environments were further characterized by more selective NMR experiments, carried out on representative samples and model compounds as summarized in Figures 6-9 and described in text below. Table I gives an overview of the samples and the species quantitation by NMR, while Table II summarizes

**TABLE I: Compositions, Surface Coverages  $\theta$ , and Relative  $^{51}\text{V}$  NMR Signal Areas of the Samples under Study**

support	$\text{V}_2\text{O}_5/\text{wt } \%$	$\theta$	signal fractn <sup>a</sup> / $\%$	
			type a	type b
$\text{TiO}_2$ (anatase)	1.0	0.08	>95	<5
	2.5	0.20	>>95	<<5
	4.0	0.32	>>95	<<5
$\text{TiO}_2$ (rutile)	1.0	0.27	65	35
	2.5	0.68	80	20
	4.0	1.08	80	20
$\text{TiO}_2$ (Degussa)	1.0	0.14	50	50
	1.8	0.25	75	25
	2.5	0.35	90	10
	4.0	0.57	95	5
$\gamma\text{-Al}_2\text{O}_3$	8.0	1.14	crystalline $\text{V}_2\text{O}_5$	
	1.0	0.05	<<5	>>95
	2.0	0.10	<<5	>>95
	4.0	0.20	<10	>90
	5.0	0.25	<10	>90
	7.5	0.38	40	60
	10.0	0.50	70	30
15.0	0.75	75	25	
20.0	1.00	85	15	

<sup>a</sup> Estimated error:  $\pm 5\%$ .

the spectroscopic observables for both catalyst materials and model compounds. Included are the MAS-NMR line positions at 7.05

(47) Ganapathy, S.; Schramm, S.; Oldfield, E. *J. Chem. Phys.* **1982**, *77*, 4360.

(48) Lapina, O. B.; Simakov, A. V.; Mastikhin, V. M.; Veniaminov, S. A.; Shubin, A. A. *J. Mol. Catal.* **1989**, *50*, 55.

(49) Zamaraev, K. I.; Mastikhin, V. M. *Colloids Surf.* **1984**, *12*, 401.

**TABLE II:  $^{51}\text{V}$  NMR Parameters of the Signal Types Observed in the Catalyst Samples under Study and of Model Compounds with Well-Defined Coordination Environments**

signal type or compd	$\delta^a/\text{ppm}$	$\delta^b/\text{ppm}$	$\delta_{\text{iso}}^c/\text{ppm}$	$\delta_{11}^d/\text{ppm}$	$\delta_{22}^d/\text{ppm}$	$\delta_{33}^d/\text{ppm}$	$t_p^e/\mu\text{s}$	coordn
type a	$-510 \pm 5$	not determined <sup>f</sup>		$-250^*$	$-330^*$	$-900^{*f}$	2.4	dist octah
type b	$-550 \pm 20$	not determined <sup>f</sup>		not determined		$f$	3.3	tetrah $Q^{(2)}$
type c	$g$	not determined <sup>f</sup>		$-200^f$	$-650$	$-720$	$g$	tetrah
$\text{V}_2\text{O}_5$	-609	-609	-609	-280	-280	$-1250^h$	$6.3^h$	sq pyramid
$\text{ZnV}_2\text{O}_6$	-517	-503	-495	$-270^*$	$-410^*$	$-920^*$	2.2	dist octah
$\text{PbV}_2\text{O}_6$	-533	-533	-533	-310	-320	-1000	$g$	dist octah
$\text{Na}_6\text{V}_{10}\text{O}_{28}^*$	-500	-495	-492	$g$	$g$	$g$	$g$	dist octah
$18\text{H}_2\text{O}$	-507	-505	-505	$g$	$g$	$g$	$g$	dist octah
	-518	-515	-513	$g$	$g$	$g$	$g$	dist octah
	-536	-535	-535	$g$	$g$	$g$	$g$	dist octah
$\text{KVO}_3$	-561	-556	-553	$-300^*$	$-500^*$	$-870^*$	3.0	tetrah $Q^{(2)}$
$\text{NaVO}_3$	-579	-577	-576	-360	-530	-840	$g$	tetrah $Q^{(2)}$
$\text{NH}_4\text{VO}_3$	-573	-571	-570	-370	-530	-830	3.1	tetrah $Q^{(2)}$
$\text{Zn}_2\text{V}_2\text{O}_7$	-625	-619	-616	$-500^*$	$-640^*$	$-720^*$	3.0	tetrah $Q^{(1)}$
$\text{Cd}_2\text{V}_2\text{O}_7$	-579	-569	-563	$-370^*$	$-660^*$	$-660^*$	2.7	tetrah $Q^{(1)}$
$\text{Pb}_2\text{V}_2\text{O}_7$	-522	-521	-521	-430	-480	-620	3.2	tetrah $Q^{(1)}$
$\text{Na}_3\text{VO}_4$	-545	$g$			csa very small		$g$	tetrah $Q^{(0)}$
$\text{Ti}_3\text{VO}_4$	-477	-477	-477		csa very small		5.8	tetrah $Q^{(0)}$
$\text{Mg}_3(\text{VO}_4)_2$	-554	-554	-554		csa very small		$g$	tetrah $Q^{(0)}$
$\text{Zn}_3(\text{VO}_4)_2$	-522	-522	-522		csa very small		4.5	tetrah $Q^{(0)}$
$\text{Pb}_5(\text{VO}_4)_3\text{Cl}$	-509	-508	-508		csa very small		3.7	tetrah $Q^{(0)}$
$\text{BiVO}_4$	-434	-427	-423	$-365^*$	$-415^*$	$-520^*$	2.2	tetrah $Q^{(0)}$
$\text{AlVO}_4$	-670	-664	-661					tetrah $Q^{(0)}$
	-746	-745	-745					tetrah $Q^{(0)}$
	-780	-777	-775					tetrah $Q^{(0)}$

<sup>a</sup> Resonance shifts determined by MAS-NMR at 7.05 T:  $\pm 1$  ppm unless specified, not corrected for second-order quadrupolar shifts. <sup>b</sup> Resonance shifts determined by MAS-NMR at 11.7 T,  $\pm 1$  ppm unless specified, not corrected for second-order quadrupolar shifts. <sup>c</sup> Isotropic chemical shifts:  $\pm 2$  ppm, taking into consideration the second-order quadrupolar correction. <sup>d</sup> Chemical shift positions of shoulders and singularities of static spectrum at 7.05 T: typical error  $\pm 10$  ppm for model compounds,  $\pm 20$  ppm for the catalyst samples. Unless marked by an asterisk, these values agree within experimental error with the principal chemical shift tensor components. <sup>e</sup> Interpolated from 0.5- $\mu\text{s}$  increments; estimated error  $\pm 0.2 \mu\text{s}$ . <sup>f</sup> Value less certain or not reported, due to peak overlap or disorder. <sup>g</sup> Not determined.

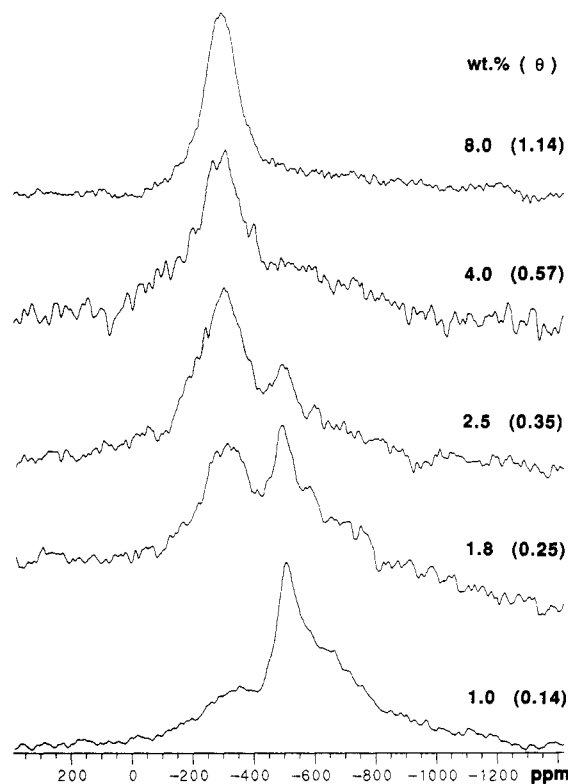


**Figure 4.** 79.0-MHz  $^{51}\text{V}$  wide-line NMR spectra of  $\text{V}_2\text{O}_5$  on  $\text{TiO}_2$  (Degussa). The numerals indicate the overall concentration and the surface coverage of  $\text{V}_2\text{O}_5$  (in parentheses.)

and 11.7 T, the isotropic chemical shifts deduced by taking into account the second-order quadrupolar correction, the pulse lengths  $t_p$  at which the signal intensities are maximized, and approximate shift values  $\delta_1$ ,  $\delta_2$ , and  $\delta_3$  that correspond to singularities and shoulders in the experimental line shape. If the nuclear electric

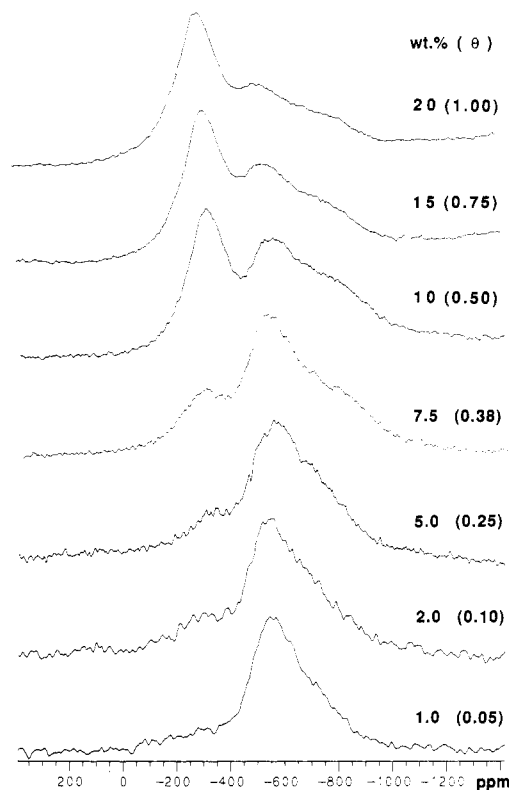


**Figure 5.** 79.0-MHz  $^{51}\text{V}$  wide-line NMR spectra of  $\text{V}_2\text{O}_5$  on  $\gamma\text{-Al}_2\text{O}_3$ . The numerals indicate the overall concentration and the surface coverage of  $\text{V}_2\text{O}_5$  (in parentheses.)

quadrupole interaction is weak, these three resonance shifts are identical with the three principal shift tensor components  $\delta_{11}$ ,  $\delta_{22}$ , and  $\delta_{33}$ .

Assuming coincident quadrupole and chemical shift tensors, Baugher et al. have given explicit algebraic expressions for these

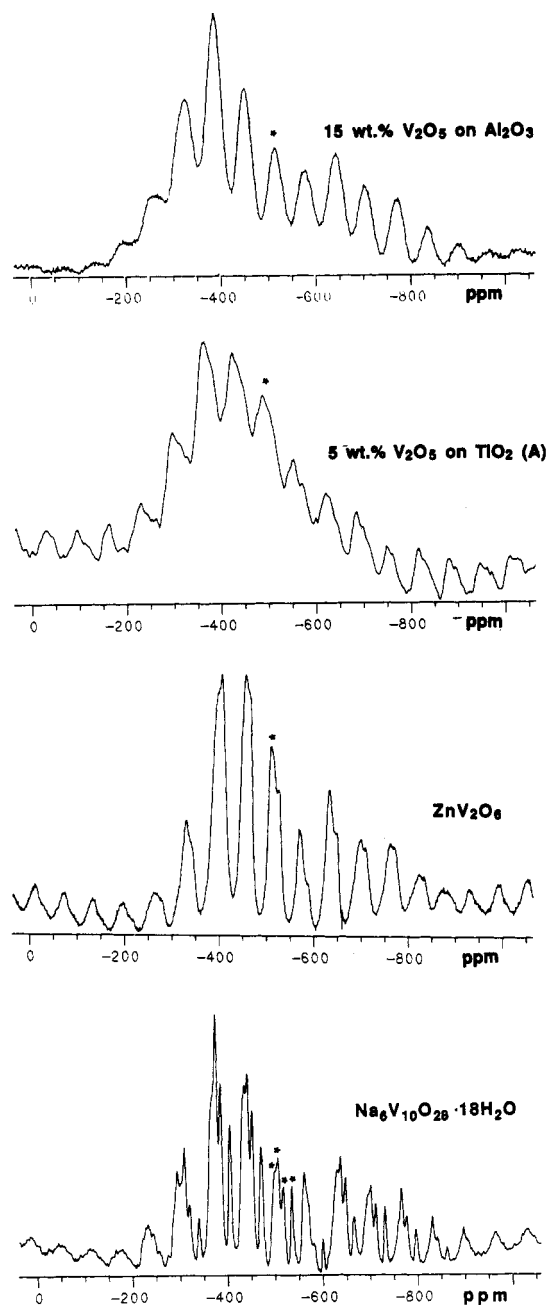


**Figure 6.** 79.0-MHz  $^{51}\text{V}$  MAS-NMR spectra of representative catalyst samples and the model compounds  $\text{ZnV}_2\text{O}_6$  and  $\text{Na}_6\text{V}_{10}\text{O}_{28}\cdot 18\text{H}_2\text{O}$ . Spinning speed ca. 5 kHz. Center bands are indicated by asterisks.

line positions.<sup>46</sup> Specifically, the largest correction due to second-order quadrupole effects arises for the most downfield feature of the chemical shift powder pattern. For a spin- $7/2$  nucleus, the position of this feature is changed (in parts per million) by the following additive term:

$$\delta^{(2)*} (\text{ppm}) = 531.4(e^2qQ/h)^2(3 + \eta)^2\nu_0^{-2}$$

For instance, if  $e^2qQ/h = 3$  MHz and  $\eta = 0$ , the correction is calculated to be ca. 7 ppm at  $\nu_0 = 79.0$  MHz, which is within the experimental error of determination. If, however, the quadrupolar interaction is considerably stronger, the experimental values  $\delta_i$  will deviate significantly from the tensor components  $\delta_{ii}$ . Since the field-dependent MAS-NMR data and the nutation spectra permit us to estimate the strength of the quadrupole coupling, we can identify those compounds for which the above restriction applies; the corresponding  $\delta_i$  values have been labeled with asterisks in Table II.

Figure 6 shows the effect of magic-angle spinning at 5 kHz. The clear MAS-NMR patterns observed for the type a signals

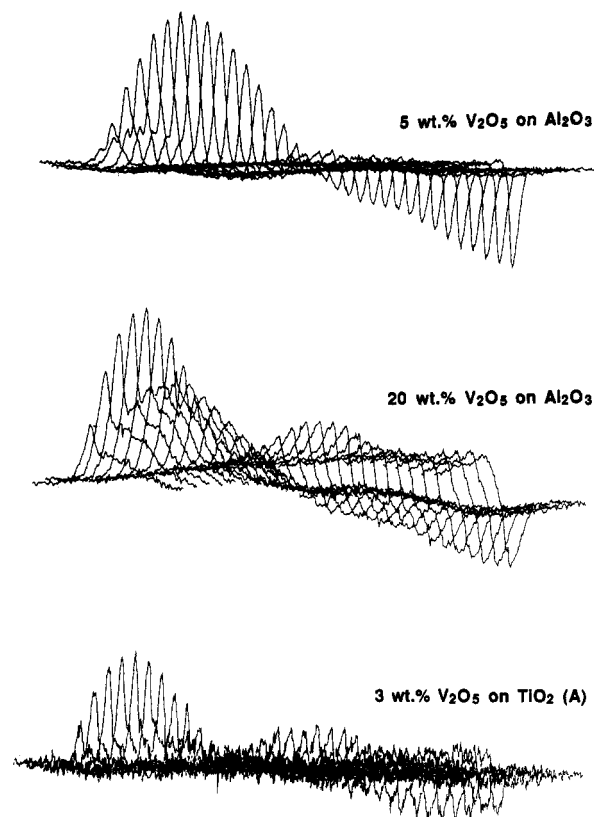


**Figure 7.**  $^{51}\text{V}$  pulse excitation behavior of representative catalyst samples at 7.05 T in a 35.7-kHz radio-frequency field. Representation is in terms of a stacked plot of normalized single Fourier transforms versus pulse length, starting with a pulse length of 0.5  $\mu\text{s}$ , up to 16  $\mu\text{s}$  in 0.5- $\mu\text{s}$  increments.

in both the anatase and the  $\gamma$ -alumina systems (see Figure 6) show the formation of a distinct, well-defined vanadium(V) oxide site, especially on  $\gamma$ -alumina at higher surface coverages. Field-dependent studies (79.0 and 131.5 MHz) show that the MAS center-band line width is approximately constant in parts per million, indicating that it is dominated by a distribution of isotropic chemical shifts. The MAS center band is located at  $-510 \pm 5$  ppm on alumina and  $495 \pm 10$  ppm on anatase; due to the inherent width and ambiguities in phasing, no reliable assessment of the second-order shift can be made. The MAS-NMR side-band patterns reveal a striking similarity to that observed in the compound  $\text{ZnV}_2\text{O}_6$ , whose spectrum is included in this figure. Note also the proximity of the center-band peak positions (see Table II). In contrast to the type a signal, MAS does not produce a clear narrowing of the type b signal in any of the samples considered, suggesting that the distribution of isotropic chemical shifts is wider than the spinning frequency. Figure 6 also includes the MAS-NMR spectra of  $\text{ZnV}_2\text{O}_6$  and  $\text{Na}_6\text{V}_{10}\text{O}_{28}\cdot 18\text{H}_2\text{O}$ . The latter compound shows four discernible peak patterns, corresponding to crystallographically inequivalent sites. The MAS-NMR peak shapes are visibly influenced by second-order quadrupolar perturbations. Note, however, the striking resemblance in the spinning side-band intensity patterns between the catalyst materials and these model compounds, as well as the proximity in the center-band positions.

Figure 7 shows the pulsed excitation behavior of representative samples. As has been shown previously for  $^{27}\text{Al}$ , this technique provides an alternative for site differentiation, purely on the basis of nuclear electric quadrupole coupling properties.<sup>50</sup> For the purpose of presentation, we prefer the  $z_1$ -domain stacked plot introduced by Man<sup>51</sup> rather than dual-frequency plots. The figure shows normalized frequency domain spectra arranged in order

(50) Janssen, R.; Tijink, G. A. H.; Veeman, W. S. *J. Chem. Phys.* **1988**, *88*, 518.

(51) Man, P. P. *J. Magn. Reson.* **1988**, *77*, 148.

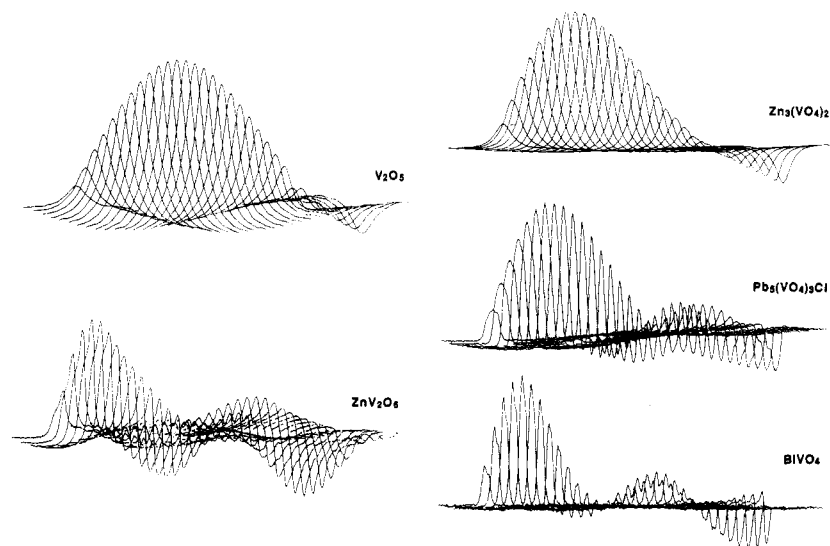


**Figure 8.**  $^{51}\text{V}$  pulse excitation behavior of several relevant model compounds at 7.05 T in a 35.7-kHz radio-frequency field. Representation is in terms of a stacked plot of normalized single Fourier transforms versus pulse length, starting with a pulse length of 0.5  $\mu\text{s}$ , up to 16  $\mu\text{s}$  in 0.5- $\mu\text{s}$  increments. The V-O bonding geometries present in these model compounds are discussed in the text and summarized in Table II.

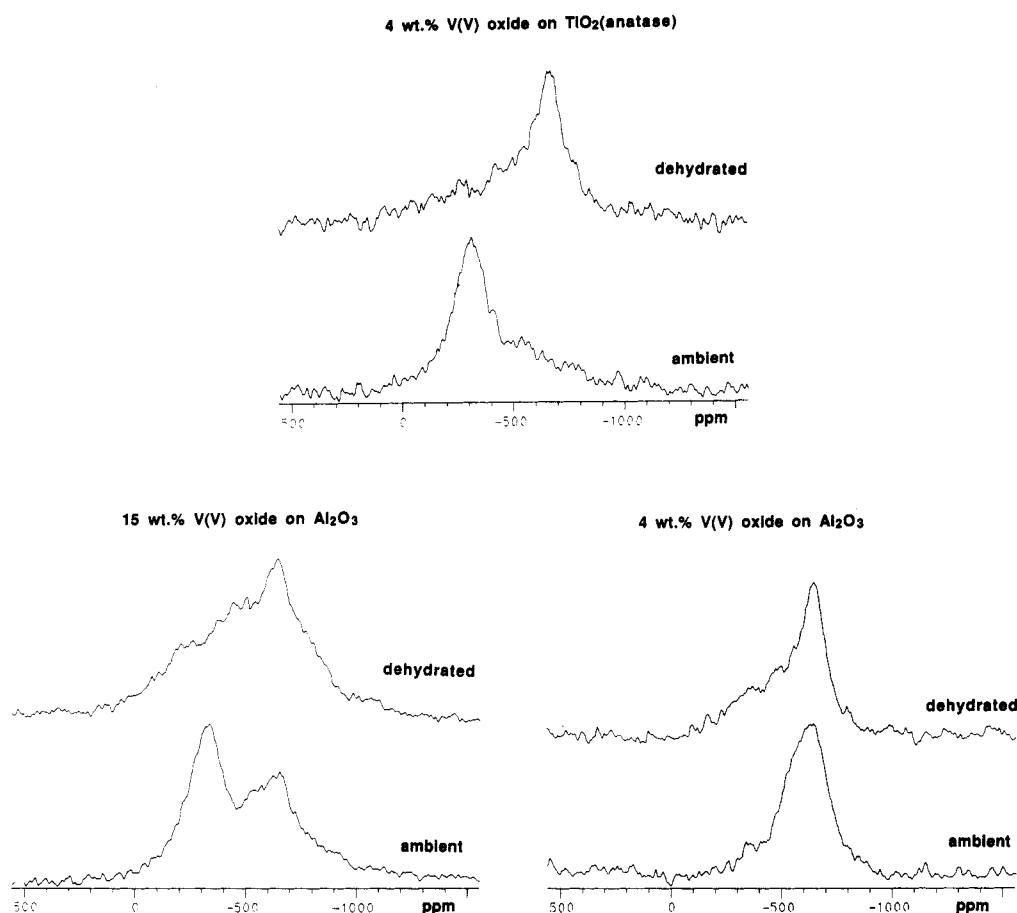


**Figure 9.** 79.0-MHz  $^{51}\text{V}$  NMR studies of representative catalyst samples under ambient conditions and in the dehydrated state.

of increasing length of the excitation pulse (from 0.5 to 16  $\mu\text{s}$  in 0.5- $\mu\text{s}$  increments). The pulse excitation experiments show that the pulse lengths that maximize the signal intensities are different for the type a and type b sites, hence providing further valuable distinction between these species. Corresponding experimental results obtained on model compounds are compiled in Figure 8. Again, the pulsed excitation behavior of  $\text{ZnV}_2\text{O}_6$  is very similar to that of the type a site in the samples.

Finally, the effect of water coordination to the surface was investigated by comparing  $^{51}\text{V}$  wide-line NMR spectra of ambient samples and samples dehydrated in vacuo at elevated temperatures

(Figure 9), as well as high-speed  $^1\text{H}$  MAS-NMR. The dehydration products of low surface coverage vanadium oxide on  $\text{TiO}_2$  (anatase) and alumina are essentially identical, whereas the spectrum of the high surface coverage alumina sample shows additional components present. The  $^1\text{H}$  MAS-NMR spectra of the ambient catalysts show very little spectroscopic discrimination between Al-OH, Ti-OH, and, conceivably, V-OH groups. From the chemical shifts observed (5–6 ppm), there is no clear evidence for sites with pronounced Brønsted acidity. The spectroscopic signature (including its dependence on spinning speeds), in conjunction with the database generated on model systems,<sup>52,53</sup>

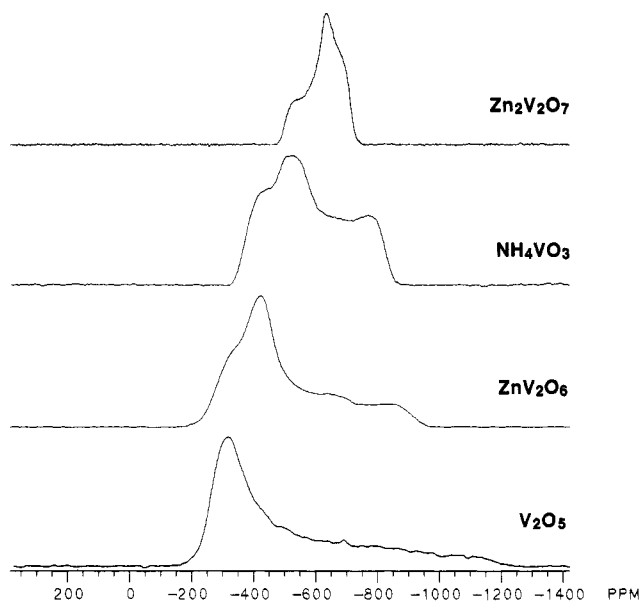


**Figure 10.** 79.0-MHz  $^{51}\text{V}$  wide-line NMR spectra of crystalline V(V) model compounds. The V–O bonding geometries present in these model compounds are discussed in the text and summarized in Table II.

suggests an assignment to mobile surface–water.

**Species Quantitation.** The spectroscopic parameters of the type a signals are very similar for all of the systems studied. Therefore, knowledge of the individual line shape of this signal from the experiments on anatase allows us to determine the vanadium(V) oxide speciation by simple difference spectroscopy; the results are included in Table I. Since the nutation NMR results show that the excitation is not entirely selective, a slight error might be expected due to partial contributions from quadrupolar first-order satellite powder patterns to the observed signal areas. In the present procedure, this error will be very small, since (a) the use of an experimental spectrum for subtracting of the type a component already includes potential satellite contributions and (b) the pulse lengths maximizing the free induction decay for both type a and type b signal components are not too dissimilar, hence implying a comparable degree of excitation selectivity. We note, however, that the use of short pulse lengths, in accordance with the condition  $t_p \leq 0.25t_{90^\circ}$  (where  $t_{90^\circ}$  is the  $90^\circ$  pulse length for nonselective excitation such as in the liquid state), is mandatory for reliable signal quantitation.<sup>41,45</sup>

**$^{51}\text{V}$  NMR Studies of Model Compounds.** To relate the  $^{51}\text{V}$  solid-state NMR spectra in the catalysts to structural information, extensive studies on vanadium(V) oxide model compounds have been carried out in our laboratory.<sup>35,54</sup> Our results, which will be published in detail separately, are summarized in Table II. A brief compilation of representative wide-line NMR spectra relevant for the interpretation of the data on the catalyst samples is given in Figure 10. Table II and Figure 10 clearly illustrate that the spectroscopic parameter that differentiates between the various tetrahedral and octahedral vanadium(V) oxide coordination environments in the most specific manner is the static NMR line shape (dominated by chemical shift anisotropy), whereas the isotropic chemical shifts alone do not provide reliable guidance. In the following discussion, we will present a correlation of these properties with local vanadium–oxygen symmetries known from the crystal chemistry of these compounds.

**5- to 6-Coordinate Vanadium.** The bonding geometry in  $\text{V}_2\text{O}_5$  is typically described as square-pyramidal, consisting of four equatorial V–O bonds of similar length and one very short axial V–O bond (1.58 Å). Alternatively, the environment could be described as 6-coordinate, if the very long (2.78 Å) second axial

V–O distance is included.<sup>55,56</sup> This coordination is reflected in a near-axially symmetric chemical shift tensor with maximized shielding along the axial direction. The wide-line spectrum shown for  $\text{V}_2\text{O}_5$  in Figure 10 was obtained on vanadium oxide prepared in microcrystalline form on a  $\text{ZrO}_2$  surface. It differs from the  $\text{V}_2\text{O}_5$  spectra previously published in the literature<sup>32–37,57</sup> by the absence of first-order quadrupolar satellites, which usually overlap with the chemical shift anisotropy powder pattern of the central transition. Presumably, the disorder present in this sample results in a spread of quadrupole coupling constants that renders these satellites unobservable, hence enabling the observation of a “cleaner” spectrum; a similar effect is evident in the top trace of Figure 4.

The bonding geometries found in the post-transition-metal metavanadates  $\text{ZnV}_2\text{O}_6$  and  $\text{PbV}_2\text{O}_6$  are substantially different from those in  $\text{V}_2\text{O}_5$  and most appropriately described as distorted octahedral.<sup>58–61</sup> In each of these compounds, there are two shorter (1.6–1.7 Å), three moderately long (1.85–2.1 Å), and one extremely long (>2.5 Å) V–O bonds. As shown in Figure 10, this bonding geometry type gives rise to a characteristic line shape quite different from  $\text{V}_2\text{O}_5$ .

Another type of 6-coordination, consisting of one short (1.6 Å), four intermediate (1.8–2.05 Å), and one long (2.2–2.3 Å) V–O bonds is present in sodium dodecavanadate,<sup>62</sup> whose MAS-NMR spectrum (Figure 6) was discussed above. Overall there is a very close correspondence in the static spectra, MAS side-band patterns, and isotropic chemical shift values for  $\text{ZnV}_2\text{O}_6$ ,  $\text{PbV}_2\text{O}_6$ , and  $\text{Na}_6\text{V}_{10}\text{O}_{29}\cdot\text{H}_2\text{O}$ . This, and the fact that none of the many 4-coordinated vanadates show such a line shape, indicates that there is a common and unique spectroscopic signature for distorted-octahedral V–O environments. It would be desirable to specify precise shielding tensor components  $\delta_{11}$ ,  $\delta_{22}$ , and  $\delta_{33}$  for this geometry. However, contrary to the case of  $\text{V}_2\text{O}_5$ , these values are not readily available from the static 79.0-MHz line shape, due to the influence of second-order quadrupolar perturbations. The fundamental differences in the nuclear electric quadrupole couplings between square-pyramidal V(V) in  $\text{V}_2\text{O}_5$  and distorted-octahedral V(V) in the compounds discussed above is evident in the field-dependent MAS-NMR peak positions. The difference is further reflected in the pulse excitation characteristics included in Figure 8 for  $\text{V}_2\text{O}_5$  and  $\text{ZnV}_2\text{O}_6$ . These experiments show near to uniform (nonselective) excitation of all transitions in the former, indicating that the nuclear electric quadrupolar interaction is weak. This finding is in good agreement with the moderately small quadrupolar coupling constant (0.805 MHz) published for  $\text{V}_2\text{O}_5$ .<sup>57</sup> In contrast,  $\text{ZnV}_2\text{O}_6$  shows maximized signal intensity at a pulse length of 2.2  $\mu\text{s}$ , revealing almost completely selective excitation of the central transition. The striking differences imply that the  $^{51}\text{V}$  nuclear electric quadrupole coupling constant of 5- to 6-coordinated vanadium(V) oxygen environments is a very sensitive indicator of local distortions.

**4-Coordinate Vanadium.** Table II indicates that  $^{51}\text{V}$  NMR is also well suited to differentiate between different types of 4-coordinated vanadates. The latter can be classified into various groups of  $Q^{(n)}$  species, according to the number of bridging oxygen atoms  $n$  that connect two different vanadium coordination polyhedra. One can distinguish  $Q^{(0)}$  species, i.e., monomeric  $\text{VO}_4^{3-}$  groups (orthovanadates);  $Q^{(1)}$  species, i.e., dimeric  $[\text{O}_3\text{V}-\text{O}-\text{VO}_3]^{4-}$  (pyrovanadates); and  $Q^{(2)}$  species, i.e., polymeric  $[\text{O}-\text{V}(\text{O}_2)]^{2-}$  (alkali metavanadates). From Table II, it is seen that, as a general

(55) Bystrom, A.; Wilhelmi, K. A.; Brotzen, O. *Acta Chem. Scand.* **1950**, *4*, 1119.

(56) Bachmann, H. G.; Ahmed, F. R.; Barnes, W. H. *Z. Kristallogr., Kristallgeom., Kristallphys., Kristallchem.* **1961**, *115*, 110.

(57) Gornostansky, S. D.; Stager, C. V. *J. Chem. Phys.* **1967**, *46*, 4959.

(58) Andreotti, G. D.; Calestani, G.; Montenero, A.; Bettinelli, M. *Z. Kristallogr.* **1984**, *168*, 53.

(59) Angenault, J. *Rev. Chim. Miner.* **1970**, *7*, 651.

(60) Angenault, J.; Rimsky, A. C. *R. Seances Acad. Sci., Ser. C* **1968**, *267*, 227.

(61) Jordan, B. D.; Calvo, C. *Can. J. Chem.* **1974**, *52*, 2701.

(62) Durif, P. A.; Averbuch-Pouchot, M. T.; Guitel, J. C. *Acta Crystallogr.* **1980**, *B36*, 680.

(52) Yesinowski, J. P.; Eckert, H. *J. Am. Chem. Soc.* **1987**, *109*, 6274.

(53) Yesinowski, J. P.; Eckert, H.; Rossman, G. R. *J. Am. Chem. Soc.* **1988**, *110*, 1376.

(54) Eckert, H.; Wachs, I. E. To be published.

rule, the differences between  $\delta_1$ ,  $\delta_2$ , and  $\delta_3$  are near zero for  $Q^{(0)}$  species, moderately small for  $Q^{(1)}$  species, and moderately large for  $Q^{(2)}$  species, for which the shielding tensor is also highly asymmetric. This close correlation with the local symmetry is in good agreement with that observed in  $^{31}\text{P}$  wide-line NMR studies of phosphates.<sup>63</sup> A finer distinction within each group of compounds is again provided by the pulse excitation NMR experiment, which proves to be a sensitive measure of local distortions specifically for  $Q^{(0)}$  compounds;<sup>54</sup> see also Figure 8.

## Discussion

On the basis of all of the above information, we can now discuss the various vanadium(V) oxide coordination environments present in the catalyst materials, in connection with the previous results obtained from competing structural techniques.

**Surface Vanadium(V) Oxide/TiO<sub>2</sub> (Anatase).** The type a signal of surface vanadium(V) oxide dominates the spectrum of all of the TiO<sub>2</sub> (anatase) samples, down to surface coverages of  $\theta = 0.08$  (1 wt % V<sub>2</sub>O<sub>5</sub>). Although these surface phases produce crystalline V<sub>2</sub>O<sub>5</sub> upon calcination at elevated temperatures, it is clear that the type a signal does not simply arise from a poorly crystallized V<sub>2</sub>O<sub>5</sub>-like precursor. Both the wide-line spectrum as well as the side-band patterns of the MAS-NMR spectrum are quite different from those of V<sub>2</sub>O<sub>5</sub>. The isotropic chemical shift of this surface species differs from that of V<sub>2</sub>O<sub>5</sub> by almost 100 ppm; in addition, the pulse excitation characteristics are quite different. The overwhelming spectroscopic evidence indicates that the vanadium oxide geometry for this species is distorted octahedral as in ZnV<sub>2</sub>O<sub>6</sub>, PbV<sub>2</sub>O<sub>6</sub>, or Na<sub>6</sub>V<sub>10</sub>O<sub>28</sub>·18H<sub>2</sub>O. Our result contrasts with the mutually contradictory conclusions drawn in ref 19 and 22, claiming V<sub>2</sub>O<sub>5</sub>-like and tetrahedral vanadium(V) oxide environments, respectively.

The spectacular line-shape change upon the dehydration of the surface (see Figure 9, top) is most striking. The spectra of the dehydrated samples indicate a change in coordination number from 6- to 4-fold, suggesting that hydrous species (OH or H<sub>2</sub>O) form part of the octahedral coordination environment in the samples under ambient conditions. The line shape is close to that expected for an axially symmetric shielding tensor, indicating the presence of higher than 2-fold symmetry. In addition, Raman studies yield a signal at 1030 cm<sup>-1</sup>, indicating an extremely short V=O bond.<sup>64</sup> While none of the model compounds investigated provide a satisfactory match to the spectrum of this "type c" species, the NMR results are compatible with formation of a  $Q^{(3)}$ -type species with a (Ti-O)<sub>3</sub>V=O environment. Unfortunately, model compounds that display this type of coordination in the solid state are not readily available.

**Surface Vanadium(V) Oxide/TiO<sub>2</sub> (Rutile).** The spectrum of vanadium(V) oxide on TiO<sub>2</sub> (rutile) shows both signal types at all surface coverages, but type a surface vanadium(V) oxide species are slightly favored at higher surface coverages. The spectroscopic characteristics of the type b signal are most consistent with a 4-fold vanadium(V) oxide species. In contrast to the TiO<sub>2</sub> (anatase) support, where this species can only be detected in traces at the very lowest surface coverages, the TiO<sub>2</sub> (rutile) support appears to stabilize 4-fold vanadium(V) oxide up to very high surface coverages. Surface dehydration at 200 °C of a sample containing 4 wt % V<sub>2</sub>O<sub>5</sub> led to the appearance of an extremely broad signal, bearing little informational content.

Our results thus indicate a striking influence of the lattice geometry of the support material upon the surface structure of vanadium(V) oxide overlayers on the different TiO<sub>2</sub> modifications, in contrast to the findings of Inomata et al.<sup>19</sup> The formation of tetrahedral surface vanadium(V) species may possibly be related to the presence of Cl<sup>-</sup> impurities or surface defects, originating from the use of TiCl<sub>4</sub> as the precursor material. Further investigations of the influence of preparative conditions upon the nature

of the vanadium(V) oxide surface species are in progress.

**Surface Vanadium(V) Oxide/TiO<sub>2</sub> (Degussa).** The results on TiO<sub>2</sub> (Degussa), which is a mixture of anatase and rutile in the ratio of 2:1, can be understood in the same fashion as the results on the rutile samples. However, the fraction of 4-coordinated vanadium(V) oxide at low surface coverage is much higher than expected from the weighted superposition of the individual spectra of vanadium(V) oxide on TiO<sub>2</sub> (anatase) and TiO<sub>2</sub> (rutile). Furthermore, the dependence on surface coverage is much more dramatic than expected. Both observations strongly suggest that at low surface coverages the rutile sites favoring 4-coordinated vanadium(V) oxide are occupied with some degree of selectivity. TiO<sub>2</sub> (Degussa) is also prepared from TiCl<sub>4</sub> at high temperature and some residual Cl<sup>-</sup> or associated defects may be responsible for stabilizing the 4-fold coordination. As, with increasing surface coverage, the number of these sites is exhausted, all of the vanadium(V) oxide is directed to octahedral sites. This model accounts well for the dramatic changes seen in the spectra of samples containing less than 3 wt % V<sub>2</sub>O<sub>5</sub>. The top spectrum in Figure 4 resembles that of crystalline V<sub>2</sub>O<sub>5</sub>, reflecting the initial stages of the formation of microcrystalline V<sub>2</sub>O<sub>5</sub>, as previously also detected by Raman spectroscopy.<sup>25</sup> As mentioned above, the first-order quadrupolar satellites are not observed, indicating the presence of some residual disorder.

**Surface Vanadium(V) Oxide/ $\gamma$ -Al<sub>2</sub>O<sub>3</sub>.** At low surface coverages, up to  $\theta$  values of ca. 0.25 (5 wt % V<sub>2</sub>O<sub>5</sub>), the "type b resonance", assigned to 4-fold surface vanadium(V) oxide dominates the spectrum. Both the asymmetry in the chemical shielding tensor and the NMR pulse excitation experiments are most compatible with a  $Q^{(2)}$  species, however, the inability to narrow this line by MAS indicates a broad range of vanadium(V) oxide environments, possibly including also differing numbers of non-bridging oxygen atoms. Although this result by itself is not very informative, Figure 5 reveals that this distribution changes very little between 1 and 5 wt % V<sub>2</sub>O<sub>5</sub>. Upon increasing the surface coverage beyond 0.25 in this system, the type a signal assigned to octahedral vanadium(V) surface oxide emerges. Detailed analysis of the spectra shows that the spectroscopic parameters for this site are independent of the surface coverage and practically identical with the spectrum seen for vanadium(V) oxide on TiO<sub>2</sub> (anatase). This is also confirmed by the more selective MAS and nutation NMR experiments (see Figures 6-8). Since the exact line shape of octahedral vanadium(V) oxide alone is known from the experiments on TiO<sub>2</sub> (anatase), we can analyze the spectra of the alumina samples quantitatively in terms of the relative amounts of octahedral and tetrahedral vanadium(V) oxide surface species present. Notwithstanding the caveat about signal quantitation discussed above, we can conclude that the most dramatic changes occur between surface coverages of 0.25 and 0.5, whereas above  $\theta = 0.5$  the fraction of the octahedral vanadium(V) oxide signal increases continuously with increasing vanadia content. Figure 9 illustrates the effect of surface dehydration at 200 °C for two representative samples. At low vanadia contents, dehydration causes a significant change in the shape but not in the general position or the center of gravity of the resonance. The line shape resembles that observed for the dehydrated vanadia on anatase sample and is consistent with 4-fold coordination of vanadium. This finding is in agreement with ref 29, which concludes on the basis of EXAFS/XANES that the tetrahedrally coordinated vanadium(V) oxide species present at low surface coverages on Al<sub>2</sub>O<sub>3</sub> is independent on the state and degree of hydration. In contrast, the vanadium(V) oxide coordination in the vanadia-rich samples is altered much more drastically upon dehydration. Although the line shape is rather complex, the comparison of Figure 9 indicates an increase in the fraction of 4-coordinated vanadium(V) surface oxide upon dehydration. Under no conditions do the NMR results show any evidence for the formation of a bulk crystalline or amorphous AlVO<sub>4</sub> phase.

## Conclusions

It is clear from the data of the present study that, at ambient conditions, as a general trend, low surface coverages favor a 4-fold

(63) Duncan, T. M.; Douglass, D. C. *Chem. Phys.* **1984**, *87*, 339.

(64) Wachs, I. E.; Jehng, J. M.; Hardcastle, F. D. *Proceedings of the International Symposium on the Reactivity of Solids. Solid State Ionics* **1989**, *32/33*, 904.

coordination of vanadium(V) oxide, whereas at higher surface coverages vanadium oxide becomes increasingly 6-coordinated. Furthermore, 4-fold coordination is the favored, but not the exclusive, bonding state in dehydrated samples. Our results also show that the chemical nature of the metal oxide support material has a marked influence. The order of increasing tendency to form 6-coordinated species at low surface concentrations (under ambient conditions) can be formulated as  $\gamma\text{-Al}_2\text{O}_3 \approx \text{TiO}_2$  (rutile) <  $\text{TiO}_2$  (Degussa) <<  $\text{TiO}_2$  (anatase).

For each system, the  $^{51}\text{V}$  solid-state NMR experiments provide detailed information about the local coordination of the two-dimensional surface vanadium oxide species on oxide supports. The structure of these surface phases depends on the surface coverage, the nature of the oxide support, and the extent of hydration. Thus, in agreement with earlier Raman and EXAFS/XANES characterization studies, the NMR experiments show that the structure of the supported vanadium oxide layer is different from that of external faces of crystalline  $\text{V}_2\text{O}_5$  and the epitaxial model based on bulk  $\text{V}_2\text{O}_5/\text{TiO}_2$  (anatase) interaction as earlier proposed.<sup>19,20</sup> At elevated temperatures (200–500 °C) required to initiate many catalytic reactions, the surface vanadium oxide phases on  $\text{TiO}_2$  predominantly possess tetrahedral coordination rather than the square-pyramidal environment present in crystalline  $\text{V}_2\text{O}_5$ .

Comparison of the  $^{51}\text{V}$  NMR and EXAFS/XANES<sup>22,24</sup> measurements of monolayer  $\text{V}_2\text{O}_5/\text{TiO}_2$  (anatase) and monolayer  $\text{V}_2\text{O}_5/\text{Al}_2\text{O}_3$  under ambient conditions suggests that there may be some difficulty with the interpretation of the EXAFS/XANES data since under ambient conditions distorted vanadia octahedra, rather than tetrahedra are predominantly present both in surface vanadium oxide monolayers on  $\text{TiO}_2$  (anatase) and  $\gamma\text{-Al}_2\text{O}_3$ . The results of the present study are in general agreement with the limited  $^{51}\text{V}$  NMR data recently reported for the  $\text{V}_2\text{O}_5/\text{Al}_2\text{O}_3$  system<sup>35,36</sup> and laser Raman spectroscopy characterization of these samples.<sup>15,25,64</sup> Thus, the new insights from the  $^{51}\text{V}$  solid-state NMR studies are greatly contributing to our fundamental understanding of supported vanadium oxide catalysts.

**Acknowledgment.** We thank Dr. H. Kung (Northwestern University) for providing us with samples of  $\text{ZnV}_2\text{O}_6$  and  $\text{Zn}_2\text{V}_2\text{O}_7$ , Dr. Pradeep Iyer (Unocal) for a sample of  $\text{Na}_6\text{V}_{10}\text{O}_{28}\cdot 18\text{H}_2\text{O}$ , and Dr. Paul Ellis (University of South Carolina) for helpful discussions. The 4.7-T NMR studies were carried out at the Southern California Regional NMR Facility, supported by NSF Grant No. 40137-84. Financial support by NSF Grant No. CBT-88107141 (I.E.W.) is gratefully acknowledged.

**Registry No.**  $\text{V}_2\text{O}_5$ , 1314-62-1;  $\text{TiO}_2$ , 13463-67-7; V, 7440-62-2.

## Thermodynamics for the Clustering of Ammonia onto $\text{Pb}^+$ in the Gas Phase

K. L. Gleim, B. C. Guo, R. G. Keese, and A. W. Castleman, Jr.\*

Department of Chemistry, The Pennsylvania State University, University Park, Pennsylvania 16802  
(Received: February 13, 1989)

Equilibrium constants together with the enthalpy, entropy, and Gibbs free energy changes were determined for the gas-phase stepwise addition reactions of up to four ammonia molecules onto the  $\text{Pb}^+$  ion. Standard enthalpy changes of  $-28.3$ ,  $-19.2$ ,  $-13.0$ , and  $-10.7$  kcal/mol and entropy changes of  $-23.3$ ,  $-27.3$ ,  $-22.0$ , and  $-24.8$  cal/K·mol were measured for the first, second, third, and fourth steps of the clustering, respectively. These results, along with earlier ones for the clustering of ammonia onto  $\text{Li}^+$ ,  $\text{Na}^+$ ,  $\text{K}^+$ , and  $\text{Rb}^+$ , provide evidence concerning the structure and types of bonding in metal ion–ammonia clusters. Since the binding in  $\text{Pb}^+\text{NH}_3$  and  $\text{Pb}^+(\text{NH}_3)_2$  is much stronger than that expected by electrostatic calculation, partial covalent interaction of  $\text{Pb}^+$  with  $\text{NH}_3$  is likely in these two clusters. Theoretical calculations were also carried out with the Sakur–Tetrode equation to determine the contributions of the translational, rotational, and vibrational components to the entropy change for each of the above clustering reactions.

### Introduction

Information on the formation and properties of cluster ions is applicable to several areas of research, including solution, nucleation, combustion, and atmospheric chemistry.<sup>1</sup> Furthermore, clusters provide a framework with which to traverse the boundary between the gaseous and condensed states.<sup>2</sup> Measurement of the thermodynamics for the formation of cluster ions yields insight into the nature of ion–molecule interactions. Moreover, thermodynamic data are essential in interpreting results from experiments involving, for instance, kinetics or photodissociation where the exothermicity of a reaction or dissociation thresholds with respect to the excess energy absorbed need to be evaluated. The present work is part of a continuing effort in our laboratory to determine the thermodynamics of the clustering of molecules onto ions via high-pressure ion source mass spectrometry. In particular, we have examined the clustering of ammonia onto  $\text{Li}^+$ ,  $\text{Na}^+$ ,<sup>3</sup>  $\text{K}^+$ ,  $\text{Rb}^+$ ,  $\text{Bi}^+$ ,<sup>4</sup>  $\text{Ag}^+$ ,  $\text{Cu}^+$ ,<sup>5</sup> and the halides.<sup>6</sup> The present

study concerns the  $\text{Pb}^+$  ion, which is also an important radon progeny.

### Experimental Section

In this study, high-pressure mass spectrometric techniques are used to investigate the thermodynamics of ion–molecule association reactions.<sup>1,2</sup> The instrument and experimental procedure have been described in detail elsewhere.<sup>3</sup> Briefly, the main components of the system are a high-pressure reaction region and a mass spectrometric sampling system (high-vacuum region). Ions are created in the high-pressure region, clustered with the desired ligands, and then extracted into the low-pressure region for mass analysis.

The ions are created thermionically within the high-pressure region by resistively heating a coated platinum filament (28 or 30 gauge) to which a positive electrical potential has been applied.<sup>7–9</sup> The coating is applied as a slurry, consisting of one part

(1) Castleman, A. W., Jr.; Keese, R. G. *Chem. Rev.* **1986**, *86*, 589.

(2) Castleman, A. W., Jr.; Keese, R. G. *Acc. Chem. Res.* **1986**, *19*, 413.

(3) Castleman, A. W., Jr.; Holland, P. M.; Lindsay, D. M.; Peterson, K. *J. Am. Chem. Soc.* **1978**, *100*, 6039.

(4) Castleman, A. W., Jr. *Chem. Phys. Lett.* **1978**, *53*, 560.

(5) Holland, P. M.; Castleman, A. W., Jr. *J. Chem. Phys.* **1982**, *76*, 4195.

(6) Evans, D. H.; Keese, R. G.; Castleman, A. W., Jr. *J. Chem. Phys.* **1987**, *86*, 2927.

(7) Kunsman, M. N. *Science* **1925**, *62*, 269.

(8) Blewett, J. P.; Jones, E. J. *Phys. Rev.* **1936**, *50*, 464.